DOI: 10.1111/jdv.15342 JEADV

REVIEW ARTICLE

Non-invasive imaging in dermatology and the unique potential of raster-scan optoacoustic mesoscopy

B. Hindelang,[1,2,3,*] J. Aguirre,[2,3,*] M. Schwarz,[2,3,4] A. Berezhnoi,[2,3] K. Eyerich,[1] V. Ntziachristos,[2,3] T. Biedermann,[1] U. Darsow[1]

[1]Department of Dermatology and Allergy, Technische Universität München, Munich, Germany
[2]Chair of Biological Imaging, Technische Universität München, Munich, Germany
[3]Institute of Biological and Medical Imaging, Helmholtz Zentrum München, Neuherberg, Germany
[4]iThera Medical GmbH, Munich, Germany
*Correspondence: B. Hindelang and J. Aguirre. E-mails: Benedikt.Hindelang@tum.de and juanaguir@gmail.com

Abstract

In recent years, several non-invasive imaging methods have been introduced to facilitate diagnostics and therapy monitoring in dermatology. The microscopic imaging methods are restricted in their penetration depth, while the mesoscopic methods probe deeper but provide only morphological, not functional, information. 'Raster-scan optoacoustic mesoscopy' (RSOM), an emerging new imaging technique, combines deep penetration with contrast based on light absorption, which provides morphological, molecular and functional information. Here, we compare the capabilities and limitations of currently available dermatological imaging methods and highlight the principles and unique abilities of RSOM. We illustrate the clinical potential of RSOM, in particular for non-invasive diagnosis and monitoring of inflammatory and oncological skin diseases.

Received: 26 June 2018; Accepted: 18 October 2018

Conflicts of interest

VN and MS have a financial interest in iThera Medical GmbH, Munich, Germany, which, however, was not involved in this work. The other authors declare no conflicts of interest.

Funding sources

The authors have received funding from the European Union's Horizon 2020 research and innovation programme under grant agreement no. 687866 (INNODERM), as well as funding from the European Research Council (ERC) through the European Union's Horizon 2020 research and innovation programme under grant agreement no. 694968 (PREMSOT) and from Deutsche Forschungsgemeinschaft (DFG) under grant agreement SFB 824, project B10.

Introduction

There is a wide range of dermatologic diseases that cannot be diagnosed or evaluated sufficiently by visual inspection alone. Histopathologic assessment of skin biopsies remains, therefore, a very important tool and diagnostic gold standard in dermatology. This is not only time-consuming and uncomfortable for the patient, but it also carries the risk of prolonged bleeding, wound infection and scar formation.[1] Therefore, high-resolution, non-invasive skin imaging techniques hold potential to make dermatological diagnostics more convenient, faster and potentially cheaper.[2] Further, because non-invasive techniques do not alter the examined tissue, the same area can be repeatedly assessed over time. This allows for better disease monitoring and more accurate evaluation of therapeutic outcomes.[3] Several high-resolution, non-invasive imaging methods have been introduced to dermatology in recent decades (Table 1). These modalities may be classified into microscopic or mesoscopic according to how deeply in the skin they can resolve clinically relevant features. Microscopic methods can be used to penetration depths shallower than 0.5–1 mm, while mesoscopic methods can penetrate deeper, as far down as 10 mm.[4]

Dermatologic imaging methods based purely on optical or ultrasound excitation

Microscopy methods

Reflectance confocal microscopy (RCM) is increasingly being used in routine clinical dermatology.[2,5] In RCM, the skin is scanned by a focused laser beam and backscattered photons are

Table 1 Technical performance characteristics of relevant dermatological imaging methods and raster-scan optoacoustic mesoscopy (RSOM)

	Reflectance Confocal Microscopy (RCM)[1,7,89]	Multiphoton Microscopy (MPM)[1,25,90]	Optical Coherence Tomography (OCT)[24,25,28,91,92]	20-MHz High-frequency ultrasound (HFUS)[34,37,93]	Raster-scan optoacoustic mesoscopy (RSOM)[33,59,94]
Contrast mechanism	Light reflection	Light Absorption	Reflection of low-coherent light	Reflection of ultrasound waves	Light Absorption
Axial resolution, μm	3–5	1	5–10, 3*	30	5
Lateral resolution, μm	0.5–1	0.3	10–15, 3*	200	20
Penetration depth, mm	0.2–0.25	0.2	1–2, 0.57* 0.5†	10	1.5 (visible light), 5 (NIR‡)
Typical field of view, mm²	0.50 × 0.50	0.35 × 0.35	6 × 6 1.8 × 1.5*	8 × 12	4 × 2§
Current state of development	Clinical practice	Clinical research	Clinical practice	Clinical practice	Clinical research

*High-definition OCT (HD-OCT).
†OCT-based angiography.
‡Near-infrared light.
§Typical field-of-view; fields up to 8 × 8 mm^2 are feasible.

detected. A pinhole is used to reject photons that arrive from out-of-focus areas.[2,6] RCM can provide sub-cellular resolution close to that of conventional histology (axial resolution, 3–5 μm; lateral resolution, 0.5–1 μm). Typically, however, imaging is restricted to depths of a few hundred micrometres (200–250 μm), corresponding to the papillary dermis or sometimes the superficial reticular dermis, owing to diminishing confocal signal with increasing depth, primarily because of light scattering.[5–7] RCM can provide valuable information in the assessment of melanocytic skin tumours. Adding RCM to dermatoscopy when diagnosing suspicious melanocytic lesions can reduce the 'number needed to treat' and thereby reduce unnecessary excisions.[2,8,9]

Multiphoton microscopy (MPM) constitutes another promising microscopic modality, although it is not yet part of routine dermatological diagnostics. MPM utilizes multiphoton excitation to generate fluorescence from tissue fluorophores (mostly NADH/NADPH, melanin, keratin and elastin) as well as harmonic signals, e.g. second-harmonic signals from non-centrosymmetric biomolecules, primarily collagen.[1,10–13] MPM achieves a lateral resolution of around 0.3 μm and an axial resolution of about 1 μm. When imaging skin, MPM is limited to a penetration depth of 200 μm.[1] MPM shows potential for early diagnosis of melanoma because it can identify conventional histology features associated with malignancy, such as disordered tissue and cell architecture and occurrence of pleomorphic or dendritic cells in the upper epidermis. In addition, MPM can detect suspected disease hallmarks invisible to light microscopy, such as poorly delineated keratinocytes. One study found MPM to be highly sensitive and specific at differentiating benign and malignant melanocytic lesions.[14,15] The ability of MPM to visualize and measure collagen content in skin[16] may facilitate assessment of skin ageing[17] and scleroderma.[18]

Both RCM and MPM are suitable only for thin and superficial lesions because light is strongly scattered as it passes through tissue. Structures situated in or extending deeper than the papillary dermis, such as many nodular melanomas, or which present distinct hyperkeratosis, often found in acral lentiginous melanomas and non-melanoma skin cancers, cannot be assessed comprehensively.[19–21] Moreover, they offer small fields-of-view of only 0.5 × 0.5 mm^2 approximately[1] and therefore often cannot image entire lesions at once. This can complicate the evaluation of structural architecture, which is often a crucial diagnostic criterion, e.g. in melanocytic lesions.[1] Stitching together smaller images into a larger one can overcome this limitation, but it is far more time-consuming than single-image acquisition.[5]

Mesoscopy methods

Mesoscopic imaging modalities compensate for light scattering, providing deeper penetration. They also typically provide larger fields of view up to several mm^2. These methods detect contrast based either on energy reflection or energy absorption. Reflection-based imaging tends to provide primarily morphological information, while absorption-based imaging resolves the distributions of specific biomolecules and can even indicate concentrations in some cases.[22] The two most important mesoscopic imaging techniques, optical coherence tomography (OCT) and high-frequency ultrasonography (HFUS),[23] are reflection-based: OCT detects reflected light, while HFUS detects reflected ultrasound.[22]

Optical coherence tomography is increasingly used in dermatological clinical practice. In OCT, the skin tissue is illuminated

with low-coherence light, and reflected photons are detected by interferometry, which allows coherence matching between the reflected light and a reference beam. This process is called coherence gating and causes multiply scattered photons to be rejected, achieving penetration down to 1–2 mm.[24,25] Conventional OCT imaging offers an axial resolution of 5–10 μm and a lateral resolution of 10–15 μm. Recently described high-definition OCT can reach a resolution of 3 μm along all axes, but penetration depth is limited to around 570 μm.[24] OCT is used for assessing whether a suspicious non-melanocytic lesion is malignant and for evaluating excision margins; in these contexts, OCT serves usually as a complementary tool when clinical inspection and dermatoscopy are inconclusive.[26,27] As a reflection-based method, OCT provides primarily morphological information,[22] since the greatest contrast is achieved at tissue interfaces. Novel flow-sensitive OCT angiography methods such as Dynamic OCT (D-OCT) can detect parts of the skin microvasculature and create overlay images with conventional morphologic OCT-images, which allows simultaneous assessment. So far they have shown potential for providing objective therapy monitoring during vasoconstrictive topical therapy of rosacea and might help in the differentiation of non-melanoma skin cancer and of its precursor lesions based on microvascular patterns.[3,28–31] A principal disadvantage of flow-sensitive OCT devices is, however, that their use is limited to depths around 500 μm, and the resulting images offer relatively little depth information because of strong artefacts in the axial direction. As a result, relevant information is mostly limited to the en face views.[24,28,32,33]

Like OCT, ultrasonography depends on contrast generated at interfaces, in this case interfaces separating media of different acoustic impedance.[34] Ultrasound waves are significantly less influenced by scattering in tissue than the light employed by OCT and other optical imaging modalities. Therefore, imaging methods based on ultrasound can generally penetrate deeper while preserving good resolution.[35,36] Nevertheless, both penetration depth and resolution depend on the frequency range at which the transducer operates. HFUS offers better axial resolution, but shallower penetration, than conventional ultrasonography. For example, HFUS using a transducer with a central frequency of 100 MHz provides axial resolution of 16 μm to a depth of 1.5 mm. HFUS at somewhat lower frequencies, which is more widely used, provides lower resolution yet can image deeper: HFUS using a transducer with a central frequency of 20 MHz can provide axial resolution of 30 μm to a depth of 10 mm.[34] The lateral resolution of clinical ultrasonography systems with 20-MHz transducers is around 200 μm.[37] A major clinical application of HFUS is the preoperative evaluation of melanoma thickness, which is important for surgery planning and tumour staging.[34,38–40] Because of difficulties in distinguishing malignant from neighbouring benign melanocytic or lymphocytic tissue, HFUS tends to overestimate melanoma thickness.[41–43] In addition, the quality of HFUS imaging is generally adversely affected by strong speckle effects, and, as a reflection-based imaging modality, it is relatively insensitive to pathophysiological properties of inflammation or angiogenesis.[44] Doppler HFUS can image skin blood flow without using exogenous contrast agents, yet such agents are required for resolving microvasculature with diameters below 100 μm.[45]

Dermatologic imaging using raster-scan optoacoustic mesoscopy

Optoacoustic imaging is based on the detection of ultrasound waves generated within the skin in response to pulsed light illumination (Fig. 1a,c). Light-absorbing biomolecules absorb the photonic energy depositing heat in the tissue which leads to thermo-elastic expansion. This expansion produces ultrasound waves, which are detected by transducers. Software is used to convert wavefront information into a 3D image reconstruction. The resulting images depict the distribution of the optical absorbers in tissue. The illumination wavelength is chosen in order to detect contrast from the desired absorber: for example, wavelengths in the visible or near-infrared range of the light spectrum can be used to detect hemoglobin, allowing the imaging of vessels.[4,46]

In recent years, several optoacoustic approaches have been tested for skin imaging. While macroscopic optoacoustic methods using broad illumination schemes and ultrasound detector arrays penetrate as deep as 3 cm and have been used for imaging larger vessels and pilot measurements of melanoma thickness, their resolution (typically 100–300 μm) is not sufficient for imaging the small dermal vasculature.[47–49] Microscopic optoacoustic devices, on the other hand, employ focused light to generate ultrasound signals from a very confined area. This allows for high-resolution imaging that resolves the superficial microvasculature. The penetration depth of such systems is, however, fundamentally limited by light scattering and, therefore, similar to that of RCM or MPM. To the best of our knowledge, microscopic optoacoustic devices have not yet entered clinical research.[46,50–53] Optoacoustic mesoscopy methods use non-focused illumination schemes in combination with a focused ultrasound detector, which enables imaging to depths of several millimetres while keeping high resolution.[54–58] A fundamental limitation of previous systems has, however, been the narrow bandwidth of the applied ultrasound detectors. The span of ultrasonic frequencies emitted by microvessels is very broad and depends on their size and depth. Therefore, an ultra-broadband acoustic detector is needed in order to resolve simultaneously small capillaries and larger dermal vessels through the entire depth of the skin. To date, only raster-scan optoacoustic mesoscopy (RSOM), which employs novel lithium niobate-based ultrasound transducers with an extended bandwidth from 10 to 180 MHz, has shown this capacity, which makes it suitable for clinical dermatological research.[33,59,60]

In RSOM, the area of interest is scanned line by line in raster mode using a single ultrasound detector combined with the

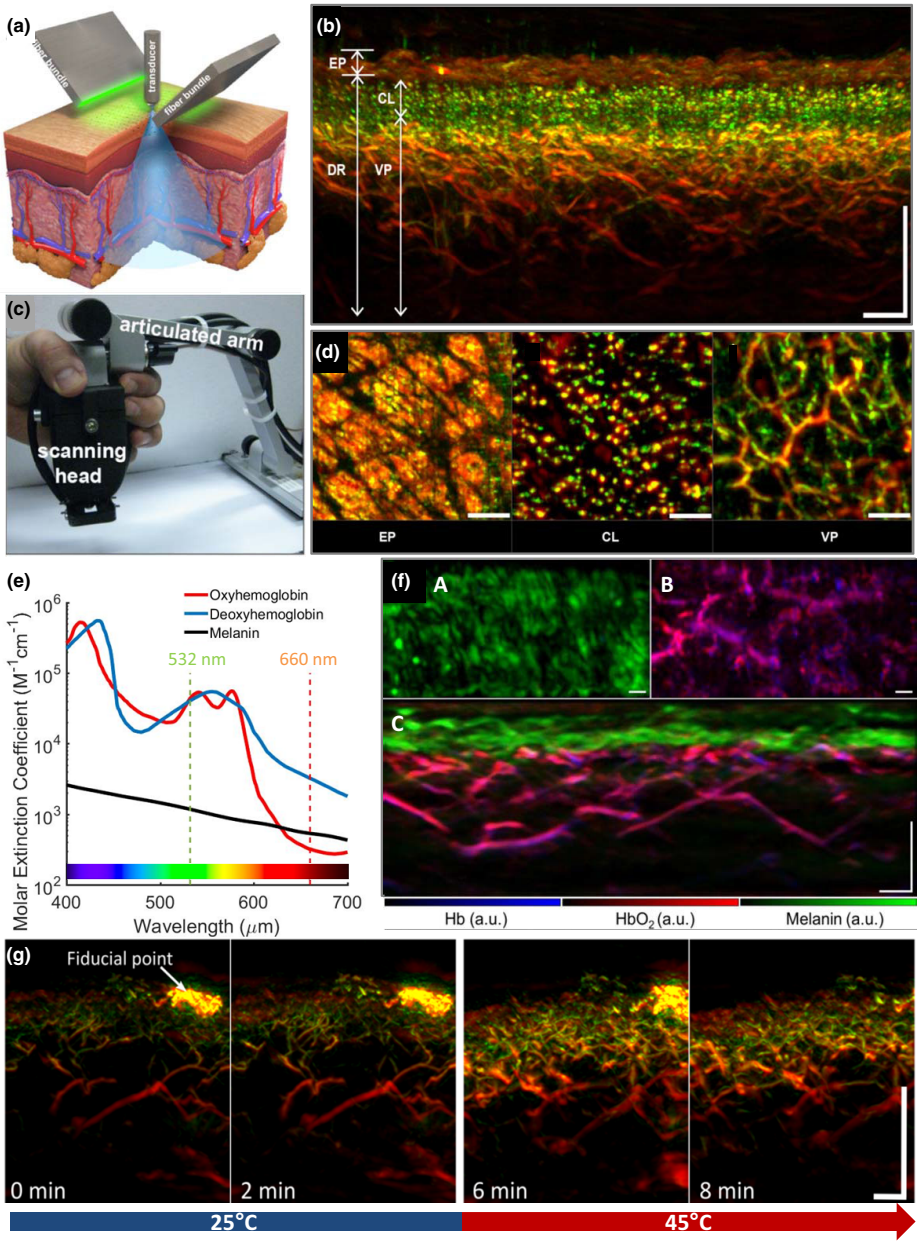

Figure 1 Raster-scan optoacoustic mesoscopy (RSOM): illustration of the system and imaging of healthy skin. (a) Schematic illustration of an RSOM system, depicting the configuration of the ultrasound detector (transducer) and the illumination bundles. (b) RSOM images of healthy skin in transverse cross section. Smaller structures (e.g. small vessels) emit ultrasound signals rich in high-frequency components (depicted in green); larger structures (e.g. larger vessels) emit signals rich in low-frequency components (depicted in red). Scale bar, 500 μm. (c) Photograph of RSOM scanning head attached to an articulated arm. (d) RSOM images of skin layers in enface sections. CL, capillary loops; DR, dermis; EP, epidermis; VP, vascular plexus. Scale bar, 500 μm. (e) Absorption spectra of melanin, oxy- and deoxyhemoglobin as a function of the wavelength of the applied light. At 532 nm, the three chromophores absorb equally strongly and therefore emit equally intense optoacoustic signals. At 660 nm, the weaker absorption by oxy- and deoxyhemoglobin allows for largely selective imaging of the skin's melanin distribution. (f) Mapping of the distribution of melanin, oxy- and deoxyhemoglobin in human skin generated through unmixing of multispectral RSOM imaging: A, en face cross section through the epidermal layer; B, en face cross section through the dermal layer; and C, transverse cross section through the entire skin. Scale bar, 250 μm. (g) Transverse cross section of forearm skin before local heating (minutes 0 and 2) and after local heating (minutes 6 and 8) from 25 to 44°C. The heating causes reactive vasodilation. Scale bar, 500 μm. Panels a–d modified from Aguirre *et al.* (2017)[33]; panel e, modified from https://omlc.org/spectra/hemoglobin/; panel f, modified from Schwarz *et al.* (2016)[61]; and panel g, modified from Berezhnoi *et al.* (2018).[63]

illumination source. Typically the field of view measures 4×2 mm^2, which significantly exceeds that of optical microscopic methods like RCM and MPM. The time needed to scan an area of this size is around 70 seconds.[33] Larger fields of view (up to 8×8 mm^2) are feasible but require longer scanning. In principle, RSOM resolution is depth-dependent in the same way as HFUS; in both cases, images are prepared from ultrasound waves. An important difference is that while HFUS employs narrowband signals (e.g. 5–20 MHz), optoacoustic waves induced in tissue by RSOM show an ultra-broadband frequency spectrum. Using lithium niobate-based transducers,[33] RSOM achieves a resolution of 20 μm in the lateral dimension and 5 μm in the axial dimension through the entire skin depth. This unprecedented performance has provided the first elaborate views of the microvascular tree of the skin, in which the smallest capillaries close to the epidermis are visible together with the larger arterioles and venules of the deep vascular plexus. In addition, small features of RSOM images can be enhanced by separately reconstructing low- and high-frequency ultrasound signals, followed by equalization of the frequency content.[33] In fact, RSOM can provide a higher ratio of resolution-to-depth for imaging dermis than any other label-free dermatological imaging method.[33]

When the skin is illuminated at a single wavelength in the visible or near-infrared range of the light spectrum, the resulting ultrasound signal comes nearly exclusively from hemoglobin and melanin, which have optical absorption coefficients orders of magnitude greater than those of other biomolecules. Optoacoustic mesoscopy can, therefore, image the vascular tree and melanin distribution with virtually no background signal, providing excellent contrast without the need for any exogenous label. Segmenting images to isolate the vascular tree is often straightforward, since melanin-rich structures usually do not overlap morphologically with vascular structures (Fig. 1b,d).[33,59] When the skin is illuminated at more than one wavelength (multispectral mode),[61,62] the distribution and relative concentration of different photoabsorbing biomolecules can be resolved. So-called spectral unmixing algorithms are used to identify the contributions of different absorbers to the overall ultrasound waves detected by the transducer. This allows assessment of the allocation of oxyhemoglobin, deoxyhemoglobin and melanin within the skin (Fig. 1e,f).[61,62]

Raster-scan optoacoustic mesoscopy penetration depth depends on the wavelength of the laser light. In the most frequently applied wavelength range of 420–570 nm, the technique can image through the entire depth of skin, penetrating approximately 1.5 mm down. Shifting the wavelengths to the red and near-infrared region of the light spectrum (570–900 nm) increases the system's penetration to as deep as 5 mm,[33,36] because tissue absorbs light more weakly at these wavelengths.

In healthy skin, RSOM images allow for an evaluation of the epidermal melanin layer, the dermal capillary loops, the underlying horizontal plexus of the dermis and deeper laying dermal vessels (Fig. 1b,d). The measured epidermal thickness correlates quite well with histology.[33]

Uniquely among dermatological imaging techniques, RSOM can, therefore, comprehensively monitor reactivity of the dermal microvasculature to local heating at single-vessel resolution (Fig. 1g).[63] The structure and function of cutaneous vasculature may reveal information about systemic disorders such as cardiovascular diseases and diabetes mellitus,[64] so RSOM may eventually improve the risk assessment in these widespread medical conditions. RSOM's ability to image epidermis morphology and vasculature down to capillary level has already been shown to deliver valuable information, which we highlight below in the context of several dermatological diseases.

Psoriasis

Aguirre *et al.*[33] demonstrated RSOM's potential to increase objectivity in the assessment of psoriasis severity. Psoriasis is a chronic autoimmune disease most commonly involving skin with multiple red plaques covered by silver scales. Because of its characteristic microscopic appearance, histology constitutes an important tool for diagnosis. Currently, quantitative evaluation of psoriasis relies mainly on subjective clinical features: the widely used Psoriasis Area and Severity Index (PASI) is calculated from the appearance of plaque thickness, lesion redness, scaling and involved percentage of the body.[65] Visual grading of these parameters lacks precision, and the score is affected by considerable inter-observer variability.[66,67] Moreover, it takes into account only superficial features and ignores inner plaque morphology and vasculature, even though angiogenesis has been identified as a major hallmark of disease progression.[68,69]

Raster-scan optoacoustic mesoscopy imaging of psoriatic plaques revealed subsurface pathological features, namely distinct skin acanthosis, dilated and elongated capillary loops and an increased diameter of the dermal vessels (Fig. 2a–g). These findings, including vessel diameters, were in accordance with histology and immunohistochemistry (Fig. 2e/f). In order to objectively measure disease severity, the authors suggested an RSOM-based optoacoustic index (OPIND) calculated from quantitative features in RSOM images that reflect the degree of inflammation and angiogenesis. These features include the thickness of the epidermis, total blood volume in the dermis, fractal number of the vascular structure, as well as density and mean diameter of the capillary loops. Preliminary work suggested good correlation between OPIND and local PASI score in single-plaque analysis (Fig. 2g). Those authors concluded that non-invasive RSOM imaging of psoriasis may help clarify the pathogenesis of the disease and monitor individual disease progression and therapeutic outcomes.[33]

Eczema

Eczema is a different type of skin inflammation largely of atopic, toxic or allergic origin and characterized by erythema, papules

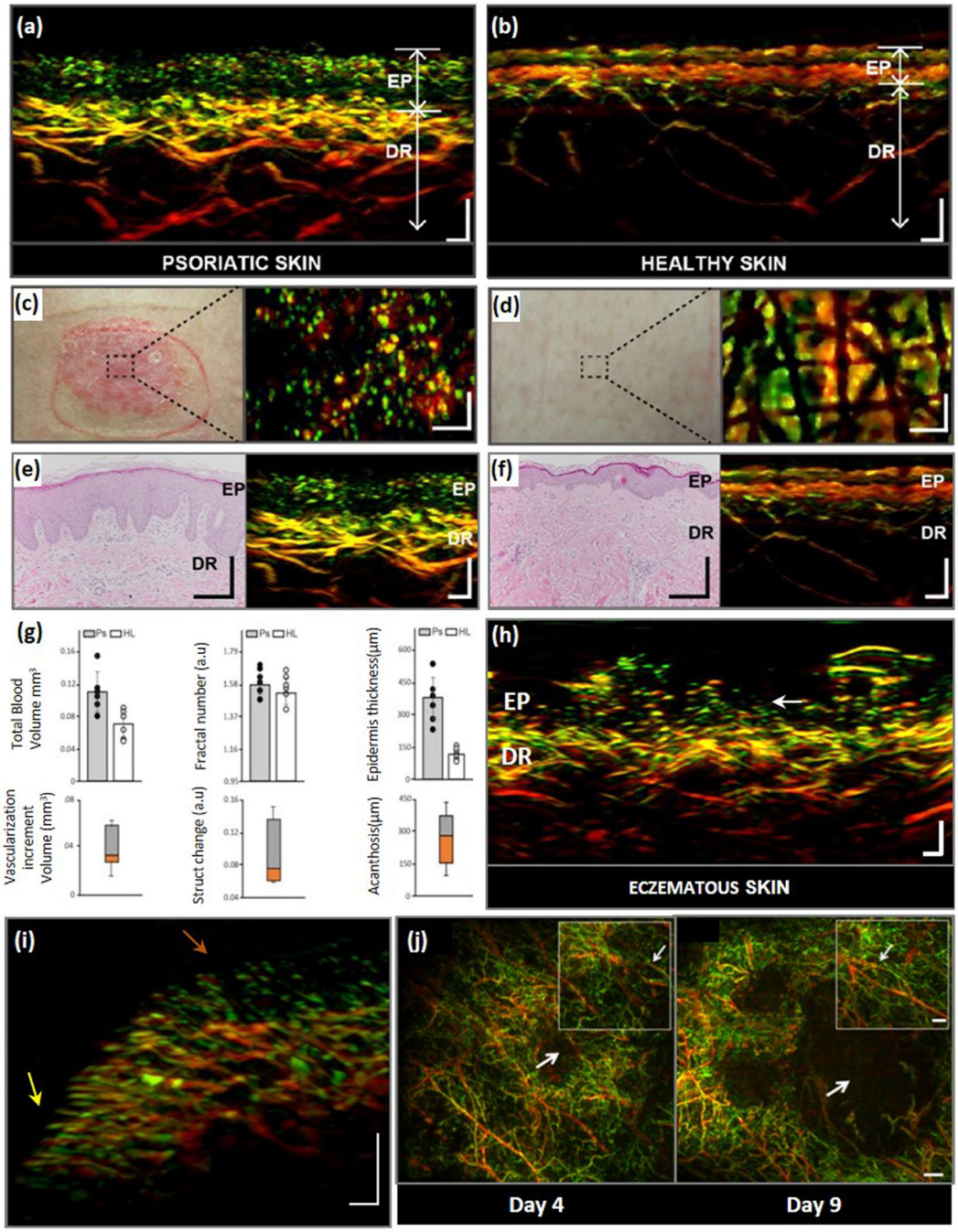

and itching, sometimes as well as blisters or lichenification. In skin affected by atopic eczema, RSOM imaging detected less acanthosis and elongation of the capillary loops than in psoriatic skin.[33] Conversely, RSOM detected prominent elongation and dilation of the capillary loops in dibromodicyanobutane-induced allergic contact eczema (clinically classified as ++ positive) (white arrow, Fig. 2h), but these loops were sparser and more irregularly distributed in contact eczema than in psoriasis. Both types of eczema presented inflammation-related changes of the dermal vasculature, especially dilation and increased vessel density.

It may be possible to derive an RSOM-based score analogous to the OPIND for quantifying features and severity of different types

Figure 2 Imaging of skin diseases using raster-scan optoacoustic mesoscopy (RSOM). (a–f) RSOM imaging comparing psoriatic plaque and adjacent healthy skin, together with the corresponding histological sections. Structures emitting high-frequency ultrasound signals (e.g. smaller vessels) are depicted in green; those emitting low-frequency signals (e.g. larger vessels) are depicted in red. (a) RSOM transverse cross-sectional image of psoriatic plaque. The elongated capillary loops (green) nearly reach the skin surface and appear interwoven with the depigmented and acanthotic epidermis (red with low contrast, EP). In the underlying dermal layer (DR), the vessels of the dermal plexus appear dilated and organized in a dense manner. Scale bar, 200 μm. (b) RSOM transverse cross section through adjacent healthy skin depicts the melanin-containing epidermis on top and the capillary loops and dermal vessels below. Scale bar, 200 μm. (c) Photograph (left) and en face RSOM image (right) of psoriatic plaque. The tips of the capillary loops appear as green dots. Scale bar, 300 μm. (d) Photograph (left) and en face RSOM image (right) of neighbouring healthy skin. The top layer of the RSOM image shows melanin-containing epidermis and physiological markings on the skin surface. Scale bar, 300 μm. (e) Histological cross section (left) and corresponding RSOM transverse cross section (right) of psoriatic skin from the location depicted in panel (c). Histology shows increased dermal vascularization, papillomatosis and elongated capillary loops. (f) Histological cross section (left) and corresponding transverse RSOM cross section (right) of healthy skin from the location depicted in panel (d). (g) Top row: Quantitative comparisons of blood volume, fractal number and epidermis thickness in psoriatic skin (Ps) and healthy skin (HL). Bottom row: Differences between measurements in psoriatic vs. healthy skin. (h) Transverse cross section of skin affected by contact eczema induced by epicutaneous allergy testing (result '++ positive'). Capillary loops (white arrow) are longer and more dilated than in healthy skin but appear more irregularly and sparsely distributed than in psoriatic skin [see panels (a) and (b)]. Vessels of the dermal plexus are dilated. Scale bar, 200 μm. (i) Transverse cross section of a skin region in close proximity to the nail fold of the fourth finger of a healthy volunteer (nail located to the left of the region shown). Yellow arrow marks capillaries that lie close to the base of the nail and are oriented parallel to the skin surface. Brown arrow highlights capillaries farther away from the nail, oriented perpendicular to the skin. Therefore, only the capillary tips are visible. Scale bar, 250 μm. (j) En face RSOM images of melanoma growth and tumour angiogenesis in subcutaneous mouse tissue captured on days 4 and 9 after injection of melanoma cells. Insets in each image depict an identical region in the immediate vicinity of the tumour: growth of smaller vasculature is visible over time between two large vessels (smaller arrow). Scale bar, 1 mm (main image), 0.5 mm (inset). Panels a–g modified from Aguirre *et al.* (2017)[33]; panel h courtesy of the authors; panel i modified from Aguirre, Hindelang *et al.* (2018); panel j modified from Omar *et al.* (2015).[36]

of dermatitis. It is notoriously difficult to distinguish mild forms of type-IV allergic reaction from irritant test reactions in epicutaneous allergy testing.[70,71] RSOM's ability to assess the microvascular structures in different skin layers[33] may facilitate such differentiation because allergic and irritant dermatitis seem to involve superficial and deep dermal vessels to different degrees.[72,73]

Scleroderma

Bright-field microscopy is an established tool for assessment of nail fold capillaries for the diagnosis of scleroderma, a chronic connective tissue disease leading to hardening of the skin and frequently affecting inner organs. This diagnostic approach is, however, limited to superficial layers of the nail fold's microvascular structure, and dry or thickened epidermis can severely compromise image quality.[74–76] RSOM, in contrast, allows for a three-dimensional assessment of the entire microvascular tree of the nail fold, including capillaries deep in the nail fold, and this ability is unaffected by the condition of the epidermis (Fig. 2i). RSOM imaging of superficial nail fold vasculature gave estimates of vessel density and capillary diameter that agreed extremely well with estimates obtained with conventional microscopy. These two parameters are widely used biomarkers of scleroderma progression.[77] RSOM's ability to depict the entire microvasculature of the nail fold holds potential for more comprehensive and reliable scleroderma assessment.

Malignant skin lesions

The high resolution of RSOM may make it effective at identifying *in situ* or early invasive melanomas. Nevocytic nevi appear as melanin-rich sections of the epidermis, and the vasculature underlying and surrounding them does not differ substantially from healthy skin vasculature based on conventional histological assessment or RSOM imaging.[36,59] RSOM may be able to detect pathological neovascularization[78,79] that occurs in the microenvironment of malignant skin tumours. Indeed, it can provide high-resolution images of angiogenesis associated with melanoma growth in mice over several days[36] (Fig. 2j). This capability may allow RSOM to facilitate diagnosis of malignant skin lesions and determination of tumour excision margins. Using OCT-based angiography it has been shown that mesoscopic analysis of vascular patterns can assist in the non-invasive detection of malignant skin lesions.[3,28,30,80] This method benefits from the simultaneous generation of conventional morphological OCT-images, which can give additional clues for diagnosis, but it lacks the capability to image deeper parts of the skin's microvasculature. Also, artefacts in the axial direction strongly compromise the depth information in OCT-based angiography (see section 'Mesoscopy methods'). Microscopic optical imaging methods like RCM and MPM can image vasculature only in thin tumours with diameters smaller than 250 μm.[1,5]

Functional RSOM imaging in skin diseases

Multispectral RSOM can image the distribution and relative concentrations of different light-absorbing biomolecules, the best established of which are melanin and oxy- and deoxyhemoglobin.[36] The ability to quantitate levels of oxy- and deoxyhemoglobin allows determination of the oxygenation status of

Table 2 Potential of relevant dermatological imaging methods and raster-scan optoacoustic mesoscopy (RSOM) to resolve selected biomarkers of important skin conditions

	Biomarkers	Reflectance confocal Microscopy (RCM)	Multiphoton microscopy (MPM)	Optical coherence tomography (OCT)	20-MHz High-frequency ultrasound (HFUS)	Raster-scan optoacoustic mesoscopy (RSOM)
Melanoma	Cellular/subcellular features (e.g. cellular atypia, pagetoid cells)	(✓) (superficial)	(✓) (superficial)	×*	×	×
	Invasion of surrounding tissue by tumour/single tumour cells	(✓) (superficial)	(✓) (superficial)	(✓) (no single cells)	(✓) (no single cells)	✓
	Neovascularization/atypical microvessels	(✓) (superficial)	(✓) (superficial)	((✓)) (partially, superficial)	×	✓
	Tumour-associated hypoxia	×	×	×	×	✓
Psoriasis/Eczema	Hyperkeratosis, acanthosis	(✓) (superficial)	(✓) (superficial)	✓	✓	✓
	Microvascular abnormalities (e.g. elongated dilated capillary loops)	(✓) (superficial)	(✓) (superficial)	(✓) (partially, superficial)	×	✓
	Cellular/subcellular features (e.g. presence of inflammatory cells, parakeratosis)	(✓) (superficial)	(✓) (superficial)	×*	×	×
Scleroderma	Microvascular abnormalities (in nail fold microvasculature and elsewhere in affected skin: e.g. giant capillaries, decrease of capillary density)	(✓) (superficial)	(✓) (superficial)	((✓)) (partially, superficial)	×	✓
	Increased dermal thickness	×	×	(✓)	✓	✓
	Sclerotic changes of dermal connective tissue (e.g. altered collagen fibres, decrease of elastic fibres)	(✓) (superficial)	(✓) (superficial)	(✓) (indirectly)	(✓) (indirectly)	×
	Local hypoxia	×	×	×	×	✓
Microvasc. dysf.†	Decreased microvascular reactivity (e.g. attenuated heat-induced vasodilation)	×	×	((✓)) (partially, superficial)	×	✓

*Novel HD-OCT reaches cellular resolution (limited to ~570 μm of penetration).
†Microvascular dysfunction, e.g. found in diabetes mellitus.

individual microvessels. For instance, one study measured average oxygen saturation of 85 ± 4% in superficial dermal vessels and 54 ± 7% in deeper dermal veins.[61] This ability may make RSOM suited to diagnosis or monitoring of hypoxia-associated dermal diseases such as systemic sclerosis,[81] as well as most types of chronic wounds.[82,83] In addition, identifying hypoxic areas may facilitate early diagnosis of many malignant cancers, including melanomas, since hypoxia plays a major role in progression and aggressiveness.[84,85] Hypoxia may also be important in melanoma resistance to chemotherapy.[86]

Research is underway to extend multispectral RSOM to other skin components such as lipids by illuminating the skin with infrared light. Lipid imaging could be useful for monitoring treatment outcomes in atopic eczema, in which the skin is lipid-depleted.[87]

Current limitations

While current RSOM devices demonstrate the potential of the technique there are still certain limitations. One current shortcoming of RSOM, when compared, e.g. to OCT, is the long scan time of about one minute for an area of 2 × 4 mm^2. OCT scans an area of 6 × 6 mm in about 30 seconds.[3,77] Longer scan times increase the risk of motion artefacts, which can occur in particular when imaging body areas strongly affected by breathing motion, such as the chest.[88] Novel advanced motion correction algorithms have been developed recently. Their implementation, together with shortened scan times due to innovative detector technologies beyond the scope of this article, is expected to improve image quality in such examinations.

Conclusion

Microscopic dermatological imaging modalities penetrate down to only a few hundred micrometres. High-resolution mesoscopic methods, which rely on contrast due to energy reflection, can penetrate deeper but provide primarily morphological information about the skin without much functional or molecular information. In addition, these mesoscopic methods at best only partially resolve the skin's microvascular structure. Uniquely among dermatologic imaging methods, RSOM combines light absorption-based contrast with deep mesoscopic penetration and an extended field of view (Table 2). Due to its novel ultra-broadband ultrasound transducer, it can resolve the comprehensive microvascular tree of the skin, and it has demonstrated clinical potential in several small studies of psoriasis, nevocytic nevi, skin inflammation and skin cancer. Besides morphological images, RSOM can provide detailed images of the distribution of oxy- and deoxyhemoglobin and potentially of other biomolecules, enabling molecular and functional imaging of skin-related and other diseases. Overall, RSOM narrows the capability gap in non-invasive dermatological imaging with great potential to resolve important biomarkers for precision medicine.

References

1 Koehler MJ, Speicher M, Lange-Asschenfeldt S *et al.* Clinical application of multiphoton tomography in combination with confocal laser scanning microscopy for in vivo evaluation of skin diseases. *Exp Dermatol* 2011; **20**: 589–594.
2 Ulrich M. Konfokale laserscanmikroskopie. *Der Hautarzt* 2015; **66**: 504–510.
3 Themstrup L, de Carvalho N, Nielsen SM *et al.* In vivo differentiation of common basal cell carcinoma subtypes by microvascular and structural imaging using dynamic optical coherence tomography. *Exp Dermatol* 2018; **27**: 156–165.
4 Ntziachristos V. Going deeper than microscopy: the optical imaging frontier in biology. *Nat Methods* 2010; **7**: 603–614.
5 Rajadhyaksha M, Marghoob A, Rossi A *et al.* Reflectance confocal microscopy of skin in vivo: from bench to bedside. *Lasers Surg Med* 2017; **49**: 7–19.
6 Kollias N, Stamatas GN. Optical non-invasive approaches to diagnosis of skin diseases. *J Investig Dermatol Symp Proc* 2002; **7**: 64–75.
7 Agozzino M, Gonzalez S, Ardigo M. Reflectance confocal microscopy for inflammatory skin diseases. *Actas Dermosifiliogr* 2016; **107**: 631–639.
8 Pellacani G, Pepe P, Casari A, Longo C. Reflectance confocal microscopy as a second-level examination in skin oncology improves diagnostic accuracy and saves unnecessary excisions: a longitudinal prospective study. *Br J Dermatol* 2014; **171**: 1044–1051.
9 Alarcon I, Carrera C, Palou J *et al.* Impact of in vivo reflectance confocal microscopy on the number needed to treat melanoma in doubtful lesions. *Br J Dermatol* 2014; **170**: 802–808.
10 Hellwarth R, Christensen P. Nonlinear optical microscopic examination of structure in polycrystalline ZnSe. *Opt Commun* 1974; **12**: 318–322.
11 Koehler MJ, Hahn S, Preller A *et al.* Morphological skin ageing criteria by multiphoton laser scanning tomography: non-invasive in vivo scoring of the dermal fibre network. *Exp Dermatol* 2008; **17**: 519–523.
12 Gannaway JN, Sheppard CJR. Second-harmonic imaging in the scanning optical microscope. *Opt Quant Electron* 1978; **10**: 435–439.
13 Friedl P, Wolf K, von Andrian UH, Harms G. Biological second and third harmonic generation microscopy. *Curr Protoc Cell Biol* 2007; **Chapter 4**: Unit 4.15.
14 Cicchi R, Crisci A, Cosci A *et al.* Time- and spectral-resolved two-photon imaging of healthy bladder mucosa and carcinoma in situ. *Opt Express* 2010; **18**: 3840–3849.
15 Dimitrow E, Ziemer M, Koehler MJ *et al.* Sensitivity and specificity of multiphoton laser tomography for in vivo and ex vivo diagnosis of malignant melanoma. *J Invest Dermatol* 2009; **129**: 1752–1758.
16 Lin S-J, Wu R Jr, Tan H-Y *et al.* Evaluating cutaneous photoaging by use of multiphoton fluorescence and second-harmonic generation microscopy. *Opt Lett* 2005; **30**: 2275–2277.
17 Koehler MJ, Preller A, Kindler N *et al.* Intrinsic, solar and sunbed-induced skin aging measured in vivo by multiphoton laser tomography and biophysical methods. *Skin Res Technol* 2009; **15**: 357–363.
18 Hahn S. Prospektive klinische Studie zur Verlaufskontrolle der systemischen Sklerodermie und Graft – versus – Host – Erkrankung unter Therapie mit extrakorporaler Photopherese mittels 20-MHz- Sonografie und Multiphotonenlasertomografie. [Dissertation]. Univ. Jena, Jena, 2010.
19 Ulrich M, Lange-Asschenfeldt S, Gonzalez S. The use of reflectance confocal microscopy for monitoring response to therapy of skin malignancies. *Dermatol Pract Concept* 2012; **2**: 202a10.
20 Calzavara-Pinton P, Longo C, Venturini M *et al.* Reflectance confocal microscopy for in vivo skin imaging. *Photochem Photobiol* 2008; **84**: 1421–1430.
21 Hashemi P, Marghoob A, Rabinovitz H, Scope A. In-vivo confocal microscopy of congential melanocytic nevi. In: Hofmann-Wellenhof R, Pellacani G, Malvehy J, Soyer HP, eds. Reflectance Confocal Microscopy for Skin Diseases. Springer-Verlag, Berlin, Germany, 2012: 115–132.
22 Omar M, Aguirre J, Ntziachristos V. Optoacoustic mesoscopy for biomedicine. *Nat Biomed Eng* 2018 (accepted).

23 von Braunmuhl T, Welzel J. Nichtinvasive bildgebende diagnostik in der dermatologie. *Der Hautarzt* 2015; **66**: 492.
24 von Braunmuhl T. Optische kohärenztomographie. *Der Hautarzt* 2015; **66**: 499–503.
25 Mogensen M, Thrane L, Joergensen TM *et al.* Optical coherence tomography for imaging of skin and skin diseases. *Semin Cutan Med Surg* 2009; **28**: 196–202.
26 Gambichler T, Pljakic A, Schmitz L. Recent advances in clinical application of optical coherence tomography of human skin. *Clin Cosmet Investig Dermatol* 2015; **8**: 345–354.
27 Schmitz L, Reinhold U, Bierhoff E, Dirschka T. Optical coherence tomography: its role in daily dermatological practice. *J Dtsch Dermatol Ges* 2013; **11**: 499–507.
28 Schuh S, Holmes J, Ulrich M *et al.* Imaging blood vessel morphology in skin: dynamic optical coherence tomography as a novel potential diagnostic tool in dermatology. *Dermatol Ther (Heidelb)* 2017; **7**: 187–202.
29 Themstrup L, Ciardo S, Manfredi M *et al.* In vivo, micro-morphological vascular changes induced by topical brimonidine studied by dynamic optical coherence tomography. *J Eur Acad Dermatol Venereol* 2016; **30**: 974–979.
30 Themstrup L, Pellacani G, Welzel J *et al.* In vivo microvascular imaging of cutaneous actinic keratosis, Bowen's disease and squamous cell carcinoma using dynamic optical coherence tomography. *J Eur Acad Dermatol Venereol* 2017; **31**: 1655–1662.
31 Themstrup L, Welzel J, Ciardo S *et al.* Validation of dynamic optical coherence tomography for non-invasive, in vivo microcirculation imaging of the skin. *Microvasc Res* 2016; **107**: 97–105.
32 Qin J, Jiang J, An L *et al.* In vivo volumetric imaging of microcirculation within human skin under psoriatic conditions using optical microangiography. *Lasers Surg Med* 2011; **43**: 122–129.
33 Aguirre J, Schwarz M, Garzorz N *et al.* Precision assessment of label-free psoriasis biomarkers with ultra-broadband optoacoustic mesoscopy. *Nat Biomed Eng* 2017; **1**: 68.
34 Jasaitiene D, Valiukeviciene S, Linkeviciute G *et al.* Principles of high-frequency ultrasonography for investigation of skin pathology. *J Eur Acad Dermatol Venereol* 2011; **25**: 375–382.
35 Vogt M, Knuttel A, Hoffmann K *et al.* Comparison of high frequency ultrasound and optical coherence tomography as modalities for high resolution and non invasive skin imaging. *Biomed Tech (Berl)* 2003; **48**: 116–121.
36 Omar M, Schwarz M, Soliman D *et al.* Pushing the optical imaging limits of cancer with multi-frequency-band raster-scan optoacoustic mesoscopy (RSOM). *Neoplasia* 2015; **17**: 208–214.
37 Sattler E. Hochfrequente sonographie. *Der Hautarzt* 2015; **66**: 493–498.
38 Bobadilla F, Wortsman X, Munoz C *et al.* Pre-surgical high resolution ultrasound of facial basal cell carcinoma: correlation with histology. *Cancer Imaging* 2008; **8**: 163–172.
39 Hayashi K, Koga H, Uhara H, Saida T. High-frequency 30-MHz sonography in preoperative assessment of tumor thickness of primary melanoma: usefulness in determination of surgical margin and indication for sentinel lymph node biopsy. *Int J Clin Oncol* 2009; **14**: 426–430.
40 Vilana R, Puig S, Sanchez M *et al.* Preoperative assessment of cutaneous melanoma thickness using 10-MHz sonography. *AJR Am J Roentgenol* 2009; **193**: 639–643.
41 Lassau N, Mercier S, Koscielny S *et al.* Prognostic value of high-frequency sonography and color Doppler sonography for the preoperative assessment of melanomas. *AJR Am J Roentgenol* 1999; **172**: 457–461.
42 Tacke J, Haagen G, Hornstein OP *et al.* Clinical relevance of sonometry-derived tumour thickness in malignant melanoma–a statistical analysis. *Br J Dermatol* 1995; **132**: 209–214.
43 Kaikaris V, Samsanavicius D, Kestutis M *et al.* Measurement of melanoma thickness – comparison of two methods: ultrasound versus morphology. *J Plast Reconstr Aesthet Surg* 2011; **64**: 796–802.
44 Gutierrez M, Wortsman X, Filippucci E *et al.* High-frequency sonography in the evaluation of psoriasis: nail and skin involvement. *J Ultrasound Med* 2009; **28**: 1569–1574.
45 Errico C, Pierre J, Pezet S *et al.* Ultrafast ultrasound localization microscopy for deep super-resolution vascular imaging. *Nature* 2015; **527**: 499–502.
46 Taruttis A, Ntziachristos V. Advances in real-time multispectral optoacoustic imaging and its applications. *Nat Photonics* 2015; **9**: 219–227.
47 Matsumoto Y, Asao Y, Yoshikawa A *et al.* Label-free photoacoustic imaging of human palmar vessels: a structural morphological analysis. *Sci Rep* 2018; **8**: 786.
48 Attia ABE, Chuah SY, Razansky D *et al.* Noninvasive real-time characterization of non-melanoma skin cancers with handheld optoacoustic probes. *Photoacoustics* 2017; **7**: 20–26.
49 Taruttis A, Timmermans AC, Wouters PC *et al.* Optoacoustic imaging of human vasculature: feasibility by using a handheld probe. *Radiology* 2016; **281**: 256–263.
50 Qin W, Chen Q, Xi L. A handheld microscope integrating photoacoustic microscopy and optical coherence tomography. *Biomed Opt Express* 2018; **9**: 2205–2213.
51 Lin L, Zhang P, Xu S *et al.* Handheld optical-resolution photoacoustic microscopy. *J Biomed Opt* 2017; **22**: 41002.
52 Park K, Kim JY, Lee C *et al.* Handheld photoacoustic microscopy probe. *Sci Rep* 2017; **7**: 13359.
53 Liu W, Shcherbakova DM, Kurupassery N *et al.* Quad-mode functional and molecular photoacoustic microscopy. *Sci Rep* 2018; **8**: 11123.
54 Chen J, Zhuo S, Chen G *et al.* Establishing diagnostic features for identifying the mucosa and submucosa of normal and cancerous gastric tissues by multiphoton microscopy. *Gastrointest Endosc* 2011; **73**: 802–807.
55 Zabihian B, Weingast J, Liu M *et al.* In vivo dual-modality photoacoustic and optical coherence tomography imaging of human dermatological pathologies. *Biomed Opt Express* 2015; **6**: 3163–3178.
56 Favazza CP, Jassim O, Cornelius LA, Wang LV. In vivo photoacoustic microscopy of human cutaneous microvasculature and a nevus. *J Biomed Opt* 2011; **16**: 16015.
57 Ford SJ, Bigliardi PL, Sardella TCP *et al.* Structural and functional analysis of intact hair follicles and pilosebaceous units by volumetric multispectral optoacoustic tomography. *J Invest Dermatol* 2016; **136**: 753–761.
58 Chen Z, Rank E, Meiburger KM *et al.* Non-invasive multimodal optical coherence and photoacoustic tomography for human skin imaging. *Sci Rep* 2017; **7**: 17975.
59 Schwarz M, Omar M, Buehler A *et al.* Implications of ultrasound frequency in optoacoustic mesoscopy of the skin. *IEEE Trans Med Imaging* 2015; **34**: 672–677.
60 Aguirre J, Schwarz M, Soliman D *et al.* Broadband mesoscopic optoacoustic tomography reveals skin layers. *Opt Lett* 2014; **39**: 6297–6300.
61 Schwarz M, Buehler A, Aguirre J, Ntziachristos V. Three-dimensional multispectral optoacoustic mesoscopy reveals melanin and blood oxygenation in human skin in vivo. *J Biophotonics* 2016; **9**: 55–60.
62 Ntziachristos V, Razansky D. Molecular imaging by means of multispectral optoacoustic tomography (MSOT). *Chem Rev* 2010; **110**: 2783–2794.
63 Berezhnoi A, Schwarz M, Buehler A *et al.* Assessing hyperthermia-induced vasodilation in human skin in vivo using optoacoustic mesoscopy. *J Biophotonics* 2018; **11**: e201700359.
64 Yvonne-Tee GB, Rasool AHG, Halim AS, Rahman ARA. Noninvasive assessment of cutaneous vascular function in vivo using capillaroscopy, plethysmography and laser-Doppler instruments: its strengths and weaknesses. *Clin Hemorheol Microcirc* 2006; **34**: 457–473.
65 Oji V, Luger TA. The skin in psoriasis: assessment and challenges. *Clin Exp Rheumatol* 2015; **33**(5 Suppl 93): S14–S19.
66 Marks R. Assessment of disease progress in psoriasis. *Arch Dermatol* 1989; **125**: 235.
67 Finlay AY, Khan GK, Luscombe DK, Salek MS. Validation of sickness impact profile and psoriasis disability index in psoriasis. *Br J Dermatol* 1990; **123**: 751–756.

68 Griffiths CEM, Barker JN. Pathogenesis and clinical features of psoriasis. *The Lancet* 2007; **370**: 263–271.
69 Ryan C, Korman NJ, Gelfand JM *et al.* Research gaps in psoriasis: opportunities for future studies. *J Am Acad Dermatol* 2014; **70**: 146–167.
70 Johansen JD, Frosch PJ, Lepoittevin J-P, eds. Contact Dermatitis, 5th edn. Springer, Berlin, 2011.
71 Fisher A, Rietschel RL, Fowler JF. Fisher's Contact Dermatitis, 6th edn. BC Decker, Hamilton, 2008.
72 Baillie AJ, Biagioni PA, Forsyth A *et al.* Thermographic assessment of patch-test responses. *Br J Dermatol* 1990; **122**: 351–360.
73 Gawkrodger DJ, McDonagh AJ, Wright AL. Quantification of allergic and irritant patch test reactions using laser-Doppler flowmetry and erythema index. *Contact Derm* 1991; **24**: 172–177.
74 Shenavandeh S, Haghighi MY, Nazarinia MA. Nailfold digital capillaroscopic findings in patients with diffuse and limited cutaneous systemic sclerosis. *Reumatologia* 2017; **55**: 15–23.
75 Hofstee HMA, Serné EH, Roberts C *et al.* A multicentre study on the reliability of qualitative and quantitative nail-fold videocapillaroscopy assessment. *Rheumatology (Oxford)* 2012; **51**: 749–755.
76 Barth Z, Witczak BN, Flatø B *et al.* Assessment of microvascular abnormalities by nailfold capillaroscopy in juvenile dermatomyositis after medium- to long-term followup. *Arthritis Care Res (Hoboken)* 2018; **70**: 768–776.
77 Aguirre J, Hindelang B, Bereznhoi A *et al.* Assessing nailfold microvascular structure with ultra-wideband raster-scan optoacoustic mesoscopy. *Photoacoustics* 2018; **10**: 31–37.
78 Mahabeleshwar GH, Byzova TV. Angiogenesis in melanoma. *Semin Oncol* 2007; **34**: 555–565.
79 Pastushenko I, Gracia-Cazaña T, Vicente-Arregui S *et al.* Squamous cell carcinomas of the skin explore angiogenesis-independent mechanisms of tumour vascularization. *J Skin Cancer* 2014; **2014**: 651501.
80 de Carvalho N, Ciardo S, Cesinaro AM *et al.* In vivo micro-angiography by means of speckle-variance optical coherence tomography (SV-OCT) is able to detect microscopic vascular changes in naevus to melanoma transition. *J Eur Acad Dermatol Venereol* 2016; **30**: e67–e68.
81 Silverstein JL, Steen VD, Medsger TA Jr, Falanga V. Cutaneous hypoxia in patients with systemic sclerosis (scleroderma). *Arch Dermatol* 1988; **124**: 1379–1382.
82 Modarressi A, Pietramaggiori G, Godbout C *et al.* Hypoxia impairs skin myofibroblast differentiation and function. *J Invest Dermatol* 2010; **130**: 2818–2827.
83 Schreml S, Szeimies RM, Prantl L *et al.* Oxygen in acute and chronic wound healing. *Br J Dermatol* 2010; **163**: 257–268.
84 Melillo G. Hypoxia and Cancer. Springer, New York, New York, NY, 2014.
85 Huber R, Meier B, Otsuka A *et al.* Tumour hypoxia promotes melanoma growth and metastasis via High Mobility Group Box-1 and M2-like macrophages. *Sci Rep* 2016; **6**: 29914.
86 Speicher PJ, Beasley GM, Jiang B *et al.* Hypoxia in melanoma: using optical spectroscopy and EF5 to assess tumor oxygenation before and during regional chemotherapy for melanoma. *Ann Surg Oncol* 2014; **21**: 1435–1440.
87 Elias PM. Lipid abnormalities and lipid-based repair strategies in atopic dermatitis. *Biochim Biophys Acta* 2014; **1841**: 323–330.
88 Schwarz M, Garzorz-Stark N, Eyerich K *et al.* Motion correction in optoacoustic mesoscopy. *Sci Rep* 2017; **7**: 10386.
89 Rajadhyaksha M, Gonzalez S, Zavislan JM *et al.* In vivo confocal scanning laser microscopy of human skin II: advances in instrumentation and comparison with histology. *J Invest Dermatol* 1999; **113**: 293–303.
90 Zieger M, Springer S, Koehler MJ, Kaatz M. Multiphotonentomographie. *Der Hautarzt* 2015; **66**: 511–521.
91 König K, Speicher M, Bückle R *et al.* Clinical optical coherence tomography combined with multiphoton tomography of patients with skin diseases. *J Biophotonics* 2009; **2**: 389–397.
92 Boone M, Jemec GBE, Del Marmol V. High-definition optical coherence tomography enables visualization of individual cells in healthy skin: comparison to reflectance confocal microscopy. *Exp Dermatol* 2012; **21**: 740–744.
93 Wilhelm K-P. Bioengineering of the Skin: Skin Imaging and Analysis, 2nd edn. Informa Healthcare, New York, 2007. (Dermatology: clinical & basic science series; vol 31).
94 Omar M, Soliman D, Gateau J, Ntziachristos V. Ultrawideband reflection-mode optoacoustic mesoscopy. *Opt Lett* 2014; **39**: 3911–3914.